Appl. Sci. **2015**, *5*, 1715-1734; doi:10.3390/app5041715

OPEN ACCESS

applied sciences

ISSN 2076-3417

www.mdpi.com/journal/applsci

Article

Electromagnetic Acoustic Transducers Applied to High Temperature Plates for Potential Use in the Solar Thermal Industry †

Maria Kogia [1,*], Liang Cheng [1], Abbas Mohimi [1,2], Vassilios Kappatos [1], Tat-Hean Gan [1,2,*], Wamadeva Balachandran [1] and Cem Selcuk [1]

[1] Brunel Innovation Centre (BIC), Brunel University, Cambridge CB21 2AL, UK; E-Mails: liang.cheng@brunel.ac.uk (L.C.); abbas.mohimi@brunel.ac.uk (A.M.); vassilis.kappatos@brunel.ac.uk (V.K.); wamadeva.balachandran@brunel.ac.uk (W.B.); cem.selcuk@brunel.ac.uk (C.S.)

[2] TWI Ltd., Granta Park, Great Abington, Cambridge CB21 6AL, UK

† This paper is an extended version of paper published in the 6th International Conference on Emerging Technologies in Non-destructive Testing (ETNDT6), Brussels, Belgium, 27–29 May 2015.

* Author to whom correspondence should be addressed; E-Mail: maria.kogia@brunel.ac.uk (M.G.), tat-hean.gan@brunel.ac.uk (T.-H.G.); Tel.: +44-778-745-5554.

Academic Editor: Dimitrios G. Aggelis

Received: 24 September 2015 / Accepted: 4 December 2015 / Published: 11 December 2015

Abstract: Concentrated Solar Plants (CSPs) are used in solar thermal industry for collecting and converting sunlight into electricity. Parabolic trough CSPs are the most widely used type of CSP and an absorber tube is an essential part of them. The hostile operating environment of the absorber tubes, such as high temperatures (400–550 °C), contraction/expansion, and vibrations, may lead them to suffer from creep, thermo-mechanical fatigue, and hot corrosion. Hence, their condition monitoring is of crucial importance and a very challenging task as well. Electromagnetic Acoustic Transducers (EMATs) are a promising, non-contact technology of transducers that has the potential to be used for the inspection of large structures at high temperatures by exciting Guided Waves. In this paper, a study regarding the potential use of EMATs in this application and their performance at high temperature is presented. A Periodic Permanent Magnet (PPM) EMAT with a racetrack coil, designed to excite Shear Horizontal waves (SH_0), has been theoretically and experimentally evaluated at both room and high temperatures.

Keywords: Electromagnetic Acoustic Transducer (EMAT); guided waves; solar thermal plants; non-destructive testing; high temperatures

1. Introduction

Solar thermal industry is an environmentally friendly means of power generation, converting solar energy into electricity. Concentrated Solar Plants (CSPs) are employed in the solar thermal industry for collecting sunlight and converting it firstly into heat and later into electricity. There are several types of CSPs such as solar towers, dish concentrators, and parabolic trough CSPs; the latter is the most widely used [1] and is shown in Figure 1a.

Figure 1. (**a**) Parabolic Trough Concentrated Plants [2]; (**b**) reflector and absorber tube [3]; (**c**) absorber Tube [4].

The two essential components of parabolic trough CSPs are the long, parabolic trough shaped reflectors and the absorber tubes. The reflector collects and focuses the sunlight to the absorber tube, which is located at the focal point of the reflector and runs its whole length. The absorber tubes are composed of long, thin, stainless steel tubes covered by a glass envelope under vacuum, as shown in Figure 1b,c. Their entire surface should be exposed to sunlight and therefore there are few access points for any extra hardware to be attached to them. Inside the tubes, working fluid, either water/molten salt or synthetic oil, is flowing, absorbing the heat of the sunlight and transmitting it into heat/steam engines for the final stages of the power generation procedure.

The high temperatures (400–500 °C), the contraction/expansion endured due to the fast cooling of the tube at high temperatures, and the vibrations can result in the appearance of defects either on the surface or inside the absorber tube. Problems with absorber tubes have been reported [5–7], such as creep, thermo-mechanical fatigue, and hot corrosion. The turbulent mixing of hot and cold flow streams of the working fluid may result in temperature variations along the pipe and consequently in thermomechanical fatigue [8–11]. Corrosion is another common problem absorber tubes may suffer from [12–14]; local pitting corrosion can cause the initiation of stress corrosion cracking or result in small-scale leaks. Most stainless steel pipes are vulnerable to pitting corrosion and stress corrosion cracking as well [15]. The low flow of the working fluid may also lead the absorber tube to overheat; consequently, the absorber tube may be subject to creep damage, thermal oxidation, softening, and/or stress rupture [16].

Non Destructive Testing (NDT) techniques are suggested to be applied for the structural health monitoring or inspection of the absorber tubes. Several NDT techniques can be used for either the inspection or the monitoring of high temperature structures; Acoustic Emission (AE), Eddy Current (EC), Holographic Interferometry, Laser Ultrasonic, Guided Wave Testing (GWT), and Infrared Thermography (IR) are some of those. These techniques have been reported for operating at temperatures up to 300 °C, though with shortcomings. Some of the drawbacks are qualitative results, sensitivity to noise, laboratorial utilization, and the need for coupling media [17–20]. AE is a passive NDT technique that has been widely deployed in Structural Health Monitoring (SHM); it monitors the elastic waves generated after the initiation or propagation of a crack [21]. Nevertheless, AE is sensitive to noise and gives qualitative results. EC is a non-contact technique that can be employed for the inspection of any electrically conductive material; however, it is subject to the skin effect, leading it to be mainly used for the detection of surface and subsurface defects [22]. Holographic Interferometry can give detailed results and be used for the detection of small defects, but it is mainly used for laboratorial tests as its setup is complicating and it is sensitive to vibrations [23]. Laser Ultrasonic has a small and adjustable footprint; therefore, it can be used for the inspection of irregular surfaces and samples of small and complex geometry. It induces high frequency ultrasound and thus very small defects can be detected as well. However, its setup is complicated and it is mainly used for laboratorial tests. GWT is used for the inspection or monitoring of large structures; mainly piezoelectric transducers are employed upon the structure being tested exciting/receiving guided waves [24]. Piezoelectric transducers require direct access to the specimen and a coupling medium (usually a water-based gel), and their response cannot travel through a vacuum. IR can be used in this application mainly for overheating identification; however, the length of the pipes makes this technique practically inefficient. The camera needs to scan the whole length of the pipe, which is time-consuming and may not be possible while the absorber tube is operating [25].

The monitoring of absorber tubes requires a non-contact NDT technique that can be applied at high temperatures without the need for a couplant and can inspect the whole length of the tube from a single point. Therefore, GWT can be applied with the use of non-contact transducers that can withstand high temperatures and excite/receive guided waves and more particularly a T(0,1) wave mode (or SH_0) [26,27]. The EMAT can be used for this application, since it is a non-contact technology that has been used in GWT and can be applied for the inspection of structures under hostile conditions such as moving specimen and elevated temperatures.

In the following section the main operating principles of EMATs are described and emphasis is also placed on the potentials and limitations of EMATs on guided waves and high temperatures. A brief description of this study follows. The results obtained from the theoretical study are shown in Section 4, where the dispersion curves of the absorber tubes were calculated and processed and a PPM EMAT with racetrack coil has been evaluated mainly regarding its guided wave purity characteristics at both room and high temperatures. In Sections 5 and 6 the experimental setup and the results of the experimental evaluation of a pair of PPM EMATs are presented. The EMATs were tested as far as their efficiency to excite SH_0 is concerned and the parameters that may affect their performance at both room and high temperatures. The EMATs were validated for their wave purity, their sensitivity to noise, their lift-off limitations, their power requirements, and their performance at high temperatures while they were exciting/receiving guided waves. Hence, a comparison between the simulated and the

experimental results is finally presented. A high temperature EMAT exciting SH_0 wave and operating up to 400–550 °C for either monitoring or long-term inspection is also to be accomplished in the near future.

2. EMAT Technology

EMAT is a non-contact technology of transducers that can be used for the inspection of moving structures or a specimen that operates at elevated temperatures. Their response can travel through a vacuum as well, making them even more suitable for this application compared to piezoelectric transducers. EMATs can excite/receive guided waves and thus they can be employed in GWT for either the inspection or the monitoring of large structures [27–30]. Hence, high-temperature EMATs may be used for the inspection or monitoring of absorber tubes. Nevertheless, the high-temperature EMATs that have been reported so far have been designed for thickness measurements [31–33]. Therefore, a high-temperature EMAT that excites/receives guided waves for the long-term inspection of high-temperature structures is still required.

A typical EMAT transducer is composed of either a permanent magnet or an electromagnet for the generation of a static magnetic field, and a coil. The coil is driven by an alternating current that generates a dynamic magnetic field. This dynamic magnetic field induces an eddy current in the specimen placed below the coil. If the specimen being tested is an electrical conductor and non-ferromagnetic, mainly Lorentz force is exerted upon the material particles; Equation (1) shows that Lorentz force is equal to the product of eddy current density and the overall magnetic field:

$$F_{\mathrm{L}} = J_{\mathrm{e}} \times (B_{\mathrm{st}} + B_{\mathrm{dyn}}) \quad (1)$$

where F_{L} is Lorentz force, J_{e} is the eddy current density, B_{st} stands for the static magnetic field, and B_{dyn} refers to the dynamic magnetic field. In this application, the absorber tubes are made of 316 L stainless steel, which is paramagnetic; therefore the main force generated in them would be Lorentz force.

The EMAT configuration and the material properties of its main components affect EMAT performance at both room and high temperatures. The material the coil is made of influences the EMAT performance. The impedance of the coil affects the energy transmitted to the specimen and the SNR/quality of the signal received; Equation (2) shows how the resistance increases with temperature rise and Equation (3) demonstrates the relationship between the temperature and the noise level of the signal received:

$$R(T) = R_0[1 + \alpha(T - T_0)] \quad (2)$$

where R_0 is the resistance of a single turn coil, α is the temperature coefficient of resistance, and T_0 is the room temperature.

$$V_{\mathrm{Noise}} = (4K\beta T R_{\mathrm{EMAT}})^2 \quad (3)$$

where K is the Boltzmann constant, T is the temperature measured in Kelvin, β is the bandwidth, and R_{EMAT} is the resistance of the EMAT coil per turn. Consequently, the coil should be preferably made of a low-resistance material such as copper. However, copper is known to oxidize at high temperatures and, therefore, other materials could be used for this application such as silver, platinum, nickel, or

constantan. Hernandez-Valle (2011) has already made an electromagnet EMAT that can operate at up to 600 °C without any cooling system for thickness measurements and apart from designing a high temperature electromagnet he has also tested several coil designs at high temperatures [32].

The permanent magnets also have limitations regarding their maximum operating temperature. The Maximum Operating Temperature (MOT) of a magnet is equal to half of its Curie Point; beyond Curie Temperature, the strength of the magnet decreases rapidly. Consequently, high Curie Point magnets are preferable for high-temperature applications. Nevertheless, the magnetic strength of the main two types of high-temperature magnets, Alnico (with a maximum operating temperature of 500 °C) and SmCo (with a maximum operating temperature of 300 °C), is smaller than the magnetic strength of Neo (NdFeB) magnets. However, NdFeB magnets cannot be used at temperatures higher than 200 °C.

A cooling system may also be required so that both the magnets and the coil will operate efficiently. Idris *et al.* have designed and tested a water-cooled EMAT that can obtain signals up to 1000 °C for thickness measurements. The EMAT was exposed to the heat source for as much time as it needed for the signal to be recorded and then it was removed [33]. Oil- and air-cooled EMATs have also been designed. Generally, the reported high-temperature EMATs seem to operate at high temperatures for short periods of time, which are suitable for inspection, but they cannot be used in long-term condition monitoring. Consequently, an EMAT operating at high temperatures (500 °C) for long periods of time is required and could be used for the structural health monitoring of high-temperature structures such as the absorber tubes.

3. Our Methodology

This study is divided into two main parts, the theoretical validation of the PPM EMAT design and the experimental evaluation of a pair of PPM EMATs. Figure 2 shows the schematic of the methodology followed in this study. In the theoretical part, the dispersion curves of a 3 mm thick, 316 L stainless steel plate were calculated for both room and high temperatures. The resonant frequency of EMAT and the wave velocity of SH_0 at the resonant frequency of EMAT for room temperature, 60 °C, 100 °C and 180 °C are also calculated. Electromagnetic simulations in COMSOL were also carried out for the theoretical validation of this EMAT design regarding its wave purity characteristics at both room and high temperatures. Experiments were conducted with a pair of PPM EMATs with racetrack coil on a stainless steel plate. During the experiments the EMATs were tested regarding their wave purity potentials, their lift-off limitations, their power requirements, and their performance at high temperatures (up to 180 °C). The results obtained from the experimental procedure were compared with the results from the theoretical validation of the EMAT and the conclusions of this study are summarized and presented in the last part of this paper.

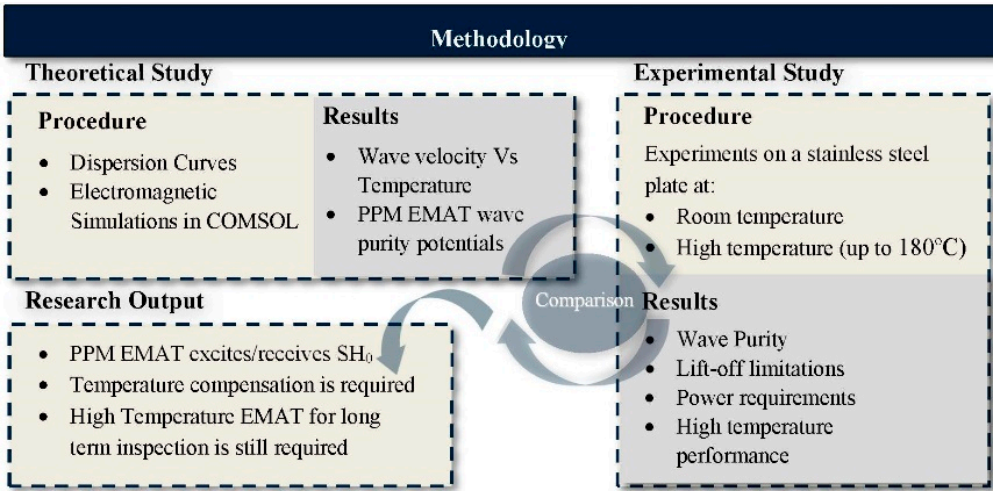

Figure 2. Methodology schematic.

4. Theoretical Study

4.1. Dispersion Curves

GWT is an NDT technique that can be employed in this applicaton. Low-frequency waves can travel big distances without being significantly attenuated; however, their relatively large wavelength limits the size of defect that can be detected. A 10 mm length of defect was set as the minimum size defect that should be detected; considering that the wavelength should be smaller than the double of the minimum size defect, in this case the wavelength should be smaller than 20 mm. A SH_0 wave of 12 mm wavelength was introduced to this structure.

As the wave propagates inside the specimen, it strikes at the boundaries of the medium, resulting in the change of its waveform. Consequently, there is an infinite number of possible wave modes that may appear in the material; their velocity changes in respect not only to the material properties of the specimen but to its geometry as well. Hence, the same mode at a different frequency may propagate with a different mode shape and velocity. This phenomenon is called dispersion; most of the wave modes in guided waves are dispersive Nevertheless, T(0,1) (or, alternatively, SH_0 on plates) is not dispersive, making the interpretation of the signal received less complicated. Its displacement is also in-plane, making it more suitable for this application, since the wave will propagate all along the pipe without it being affected by the working fluid that flows inside the pipe; T(0,1) cannot propagate in liquids. The number of wave modes that may appear in a plate is also smaller compared to a pipe and therefore the interpretation of the signal received from a plate may be less complicated as well.

In this preliminary study, the EMAT is simulated and designed for exciting SH_0 waves, which will propagate axially on a 316 L stainless steel plate. The dispersion curves of a 3 mm thick, 316 L stainless steel plate of 8000 kg/m^3 density, 195 GPa Young's modulus, and 0.285 Poisson ratio have been calculated and demonstrated in Figure 3. This figure shows that the wavelength curve crosses the SH_0 curve at 256 kHz frequency and thus this should be the resonant frequency of the EMAT. The wavelength curve also crosses the S_0, A_0, and A_1 curves; Table 1 shows at which frequency the wavelength curve crosses each wave mode curve and their wave velocity at these frequencies. Hence, an EMAT designed to excite SH_0 of 12 mm wavelength should be driven with an AC current of

256 kHz frequency. Otherwise if the EMAT is tuned to any other frequency, it will be likely for it to excite Lamp waves instead of SH_0. This is more possible if the coil design is meander instead of racetrack, for meander coils are used for Lamp waves as well. At 256 kHz, the SH_0 and the A_0 have the same group velocity. As a result, both wave modes can be excited/received from the EMAT, simultaneously resulting in a more complicated signal, since A_0 is dispersive at this frequency. Nevertheless, the orientation of the displacement of each wave mode is different; the SH_0 has an in-plane displacement while the A_0 has an out-of-plane displacement. Thus, a further study should be conducted regarding the wave mode, and more particularly the displacement to which the PPM EMAT is sensitive. Consequently, an electromagnetic simulation calculating and showing the amplitude and the direction of the wave modes generated by a PPM EMAT is needed.

Material properties such as the Young's Modulus, Poisson ratio, and density of a specimen change with temperature rise as well, resulting in variations in the velocity of the propagating wave mode. The Young's modulus and density of the specimen decrease with an increase in temperature, while the Poisson ratio increases. These changes result in a decrease in the velocity of the SH_0. Table 1 summarizes the wave velocity of SH_0, S_0, A_0, and A_1 at room temperature, 60 °C, 100 °C, and 180 °C. Hence, as the temperature rises and the wave velocity decreases, any reflections received from the EMAT should shift in time. Hence, the temperature should be kept stable during the inspection or temperature compensation should take place during the signal interpretation.

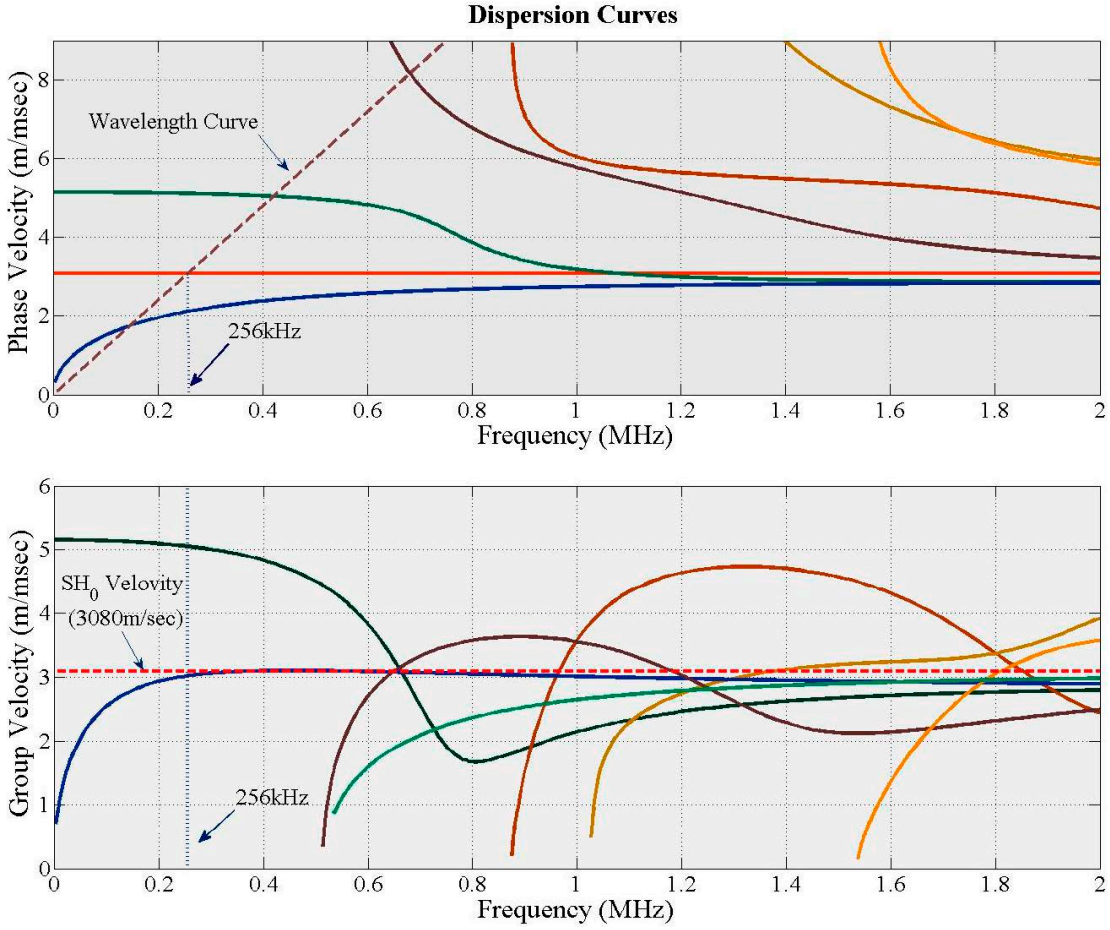

Figure 3. Dispersion curves of a 3 mm thick 316 L stainless steel plate.

Table 1. Dispersion Curves, wave velocity, and frequency.

Dispersion Curves—$SH_0/S_0/A_0/A_1$ Frequency & Wave Velocity								
Value	**Frequency (kHz)**				**Velocity (m/s)**			
Temperature (°C)	22	60	100	180	22	60	100	180
SH_0	256	255	254.2	250.6	3080	3067	3051	3008
S_0	420	419	415.5	405	5044	5022	5003	4944
A_0	143	140	139	136	1736	1720	1711	1685
A_1	676	673	668	657	8243	8217	8203	8129

4.2. Electromagnetic Simulations

Both the coil design and the magnet configuration affect the distribution of Lorentz force in space, its direction, and its amplitude. As a result, the wave mode the EMAT is to generate and/or receive gets affected by the configuration of its two main components. An EMAT configuration that can be used for the SH_0 is the PPM EMAT with racetrack coil [26–40].

In a PPM EMAT, the distance between two adjacent magnets whose magnetic field has the same direction (pitch) is equal to the wavelength; the arrangement of the magnets is illustrated in Figure 4. Racetrack coil is also used in this EMAT configuration. In this coil design there are no gaps within its turns, resulting in its broadband response in frequency. Hence, only the magnets' arrangement and the frequency of the AC current can affect the frequency response of EMAT.

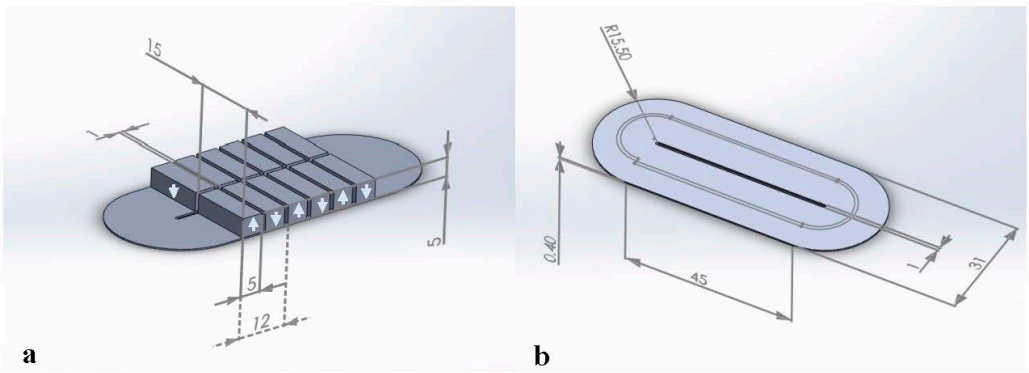

Figure 4. (**a**) Magnet arrangement in a PPM EMAT; (**b**) racetrack coil.

Finite Element Analysis (FEA) was used for the theoretical validation of this EMAT design regarding its guided wave purity characteristics at room temperature and at 180 °C. A coupled electromagnetic and mechanical analysis was carried out in COMSOL. A 3D model was created, in which a 12-magnet PPM EMAT was evaluated regarding eddy current, magnetic flux, and Lorentz force distribution. In this model two arrays of six Nd-Fe-B magnets each was simulated; each magnet has a 15 mm width, 5 mm depth, 5 mm height, and magnetization of 750 kA/m, and the direction of their magnetic flux is on the *z* axis. Their arrangement in space is the same as Figure 4 and, thus, the distance between one another is 1 mm. Due to the high requirements in time and computational power these complicated models have, the copper coil has been simplified and designed as two rectangular blocks of 35 mm width, 15 mm depth, and 0.4 mm height. The AC current driven to the coil is a two-cycle, Hanning windowed sinusoidal wave of 20 A amplitude and 256 kHz central frequency with

direction on the *x* axis. The orientation of the excitation current flowing inside one rectangular coil is opposite to the orientation of the current inside the other coil. The EMAT has a lift-off of 0.6 mm from the specimen, which is a 316 L stainless steel plate of 3 mm thickness, 750 mm width, and 750 mm depth and of the same material properties as the plate simulated in the previous section at room temperature and at 180 °C. The material, magnetic, and electrical properties of the EMAT did not change with temperature.

Figure 5a,b show the excitation/eddy current at 4 μs and the static magnetic flux distribution, respectively. Both the electric and the magnetic field are uniformly distributed. The orientation of the eddy current alters between the two sides of the coil and it is on the *x*–*y* plane. The orientation of the magnetic field alters as it is depicted in Figure 5b; its orientation is mainly on the *z* axis and its maximum strength is observed at the center of each magnet separately, as is expected. Thus, the Lorentz force generated should mainly result in an in-plane displacement. A probe was also placed 30 cm away from the EMAT for obtaining the in-plane (*x*–*y* plane) and out-of-plane (*x*–*z* plane) displacement. Figure 5c shows that the in-plane displacement maximizes at 98 μs while the out-of-plane displacement maximizes at 100 μs; the Time of Flight (ToF) of the in-plane displacement matches with the wave velocity of the SH_0, as was calculated from the dispersion curves. while the out-of-plane displacement can be the A_0. Hence, this EMAT configuration may excite the A_0 wave mode as well. However, the maximum value of the out-of-plane displacement is significantly smaller than the in-plane displacement and therefore experimental validation of this EMAT design regarding its guided wave purity characteristics is still required.

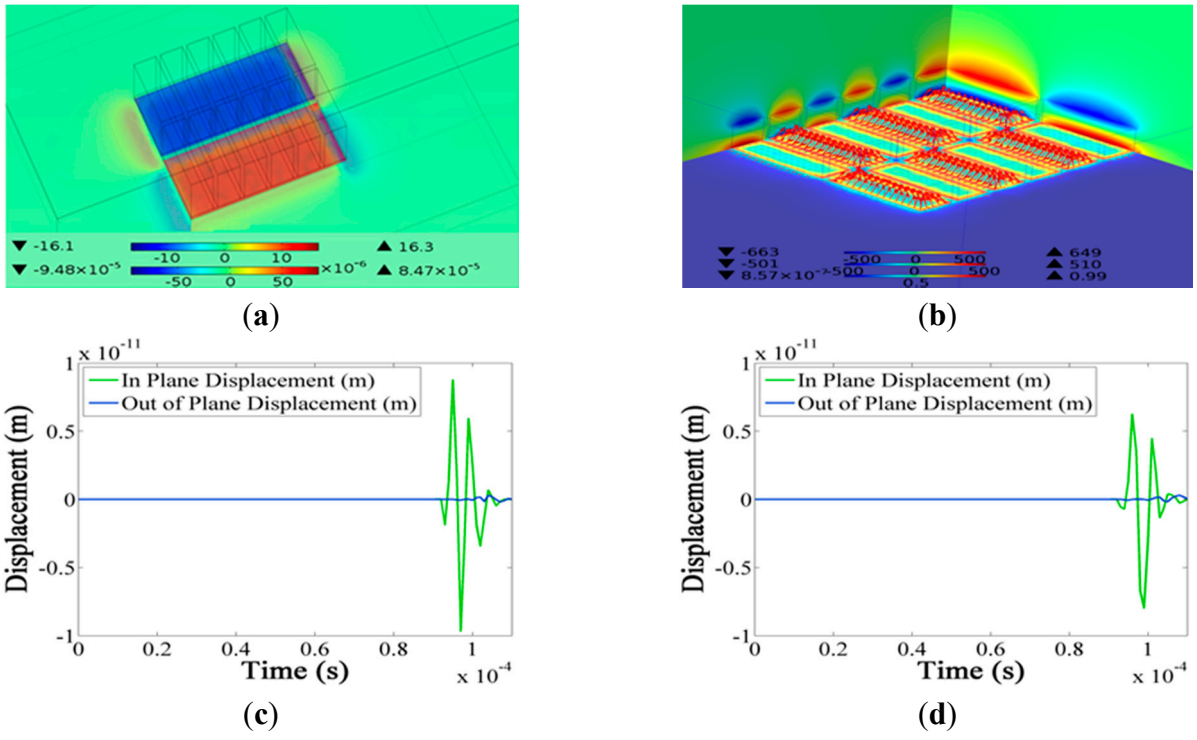

Figure 5. (**a**) Excitation/eddy current distribution at 12 μs; (**b**) magnetic flux distribution of the 12 Nd-Fe-B; (**c**) in-plane/out-of-plane displacement 30 cm away from the EMAT at room temperature; (**d**) in-plane/out-of-plane displacement 30 cm away from the EMAT at 180 °C.

Figure 5d shows the in-plane and out-of-plane displacement 30 cm away from the EMAT at 180 °C; both displacements are shifted in time, as was expected since the wave velocity changes with temperature rise and the ToF matches with the wave velocity as it was calculated from the dispersion curves. The amplitude of the in-plane displacement decreased; however, the amplitude of the out-of-plane displacement did not decrease with the temperature rise. As was mentioned, in the FEA model only the material properties of the specimen changed so that the effect of the temperature rise would be simulated. Nevertheless, the temperature rise affects the components of the EMAT as well, as was mentioned in the introduction, and thus a further decrease in the amplitude of both displacements may be observed in the experimental results, which the current model does not take into account.

Consequently, this EMAT configuration can mainly generate in-plane displacement (SH_0); however, it may also generate a small out-of-plane displacement (A_0) at this specific frequency. This can result in complicating signal analysis, since the out-of-plane displacement can be dispersive and mode conversion can also occur, which can lead to incorrect conclusions regarding the structural integrity of the specimen. In GWT, EMATs should excite a single wave mode, so that the signal received from the specimen can provide valid information regarding the structural integrity of the specimen. Also, the temperature rise affected the ultrasonic response of the EMAT, as was expected; amplitude attenuation and shifting in time were the main two changes in the signal received as the temperature increased. Hence, the wave purity characteristics of the PPM EMAT for GWT are of great importance for this application as well as the effect of temperature on the ultrasonic response of EMATs and thus an experimental validation of this EMAT design regarding its guided wave characteristics and its high-temperature performance is still required. The simulation results will be compared with the experimental results.

5. Experimental Setup

A pair of PPM EMATs with racetrack coil, manufactured by Sonemat Limited (Warwick, UK), was experimentally evaluated at both room and high temperatures. The pitch of the magnets is 12 mm and equal to the wavelength of the SH_0 [41]. During these experiments, the EMATs were tested regarding defect detection using guided waves at both room and high temperatures. Their sensitivity to noise was also experimentally evaluated; the influence of common mode noise on their performance and the effect of common ground connection between the EMAT and the specimen on the noise reduction were tested. Their lift-off limitations were validated; the thickness of the glass envelope, under which is the stainless steel pipe of the absorber tubes, will attenuate the signal generated by the EMAT and will perform as a fixed lift-off between the EMAT and the stainless steel pipe. Hence, the maximum lift-off EMATs can reach when they are used for GWT needs to be known. Their power requirements were also investigated, since only Lorentz force is generated in stainless steel, making the EMATs less efficient and more power demanding.

The experimental setup used is shown in Figure 6. The specimen used is a 316Ti stainless steel square plate of 1.25 m length and 3 mm thickness. The EMAT coil is made of lacquered copper wires of 0.315 mm diameter and the maximum operating temperature of the EMATs is 250 °C. Ritec RAM 5000 SNAP pulser/receiver (RITEC Inc., Warwick, RI, USA) was used for driving the EMAT transmitter

with a six-cycle, Hanning-windowed pulse of 256 kHz frequency. Ritec was also used for amplifying the signal received with a gain of 80 dB and filtering it within the bandwidth of 10 kHz and 20 MHz. The signal is finally collected, averaged, and recorded in a 2-channel Agilent oscilloscope (Keysight Technologies Inc., Santa Rosa, CA, USA).

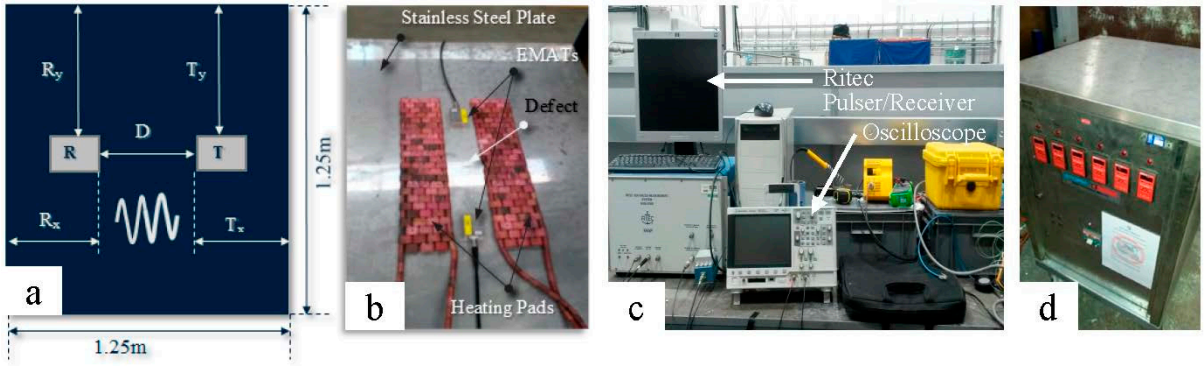

Figure 6. (**a**) Schematic of experimental setup; (**b**) experimental setup (EMATs, specimen, heating pads); (**c**) pulser/receiver—oscilloscope; (**d**) heating unit.

During the room-temperature experiments both defect-free and defective areas were tested. The distance between the transmitter and the receiver was equal to 30 cm. Five defects were created with different length and mass loss each and located 10 cm away one from the other. The defect tested was 20 mm long and with 66.6% mass loss; the transmitter was 15 cm away from one edge of the defect and the receiver was 15 cm away from the other edge of the defect. The effect of the voltage difference between the EMAT and the specimen on the quality of the signal received has been also investigated; in fact, an additional thin, stainless steel cover was also placed all around the transducers, touching both the EMATs and the specimen, for establishing a common ground connection. The influence of lift-off on EMAT response was investigated from zero to 1 mm lift-off with a step of 0.1 mm. A study regarding the power supply requirements of these EMATs was also accomplished by gradually decreasing the power output of Ritec with a step of 5% starting from its maximum power level (5000 W) and stopping at 20% of its maximum power, where no useful information could be retrieved anymore from the signal received. For the high-temperature experiments, the distance between the transmitter and the receiver was equal to 30 cm with the defect located 15 cm away from the transmitter and 15 cm away from the receiver as well (similar to the room temperature setup). The temperature was increased from ambient to 180 °C with a step of 10 °C, using a three-phase heating unit. During the high-temperature experiments the EMATs were continuously in contact with the specimen.

6. Experimental Results and Discussion

6.1. Room Temperature Experiments

During this set of experiments, the EMATs were tested for their sensitivity to common mode noise. Four case studies were investigated; the EMATs were employed in both a defect-free and a defective area, with and without common ground connection with the specimen (shielding). More particularly,

the connection/interaction between the EMAT and the specimen is differential, since the specimen induces to the EMAT coil an alternating, differential mode current. Parasitic capacitance exists between the specimen and the EMAT as a result of their physical spacing and the presence of dielectric between them [35]. Tranformers perform in a similar way and they also suffer from common mode noise; in real transformers, a small capacitance links the primary to the secondary winding and also serves as a path for the common mode current across the transformer. As a result, in both cases the common current flows to the ground via the parasitic capacitance and thus no current flows to the EMAT coil/specimen or secondary winding. Nevertheless, an autotransformer acts as a high-value parallel impedance that does not attenuate the differential current significantly but presents zero impedance to the common mode signals by shorting them to ground potential [42]. Autotransformers have smaller resistance and leakage reactance compared to conventional two winding transformers; therefore, the former is more efficient than the latter [43]. Hence, if we presume that the interaction between the EMAT and the specimen is equivalent to a transformer and we connect them so as to perform as an autotransformer, then the common mode noise should be cancelled and the EMAT receiver should work more efficiently. In this case, the alternating, differential mode current will be induced to the EMAT coil and the signal received will have an enhanced SNR and valid information would be retrieved from it. The autotransformer connection is also more robust, reasulting in an increase of the amplitude of the "wanted" signal. If an extra layer of stainless steel is attached to EMATs, touching both the EMAT housing and the specimen, then a common ground connection (autotransformer) is established. Figure 7 shows the equivalent electrical circuit of the EMAT/specimen connection.

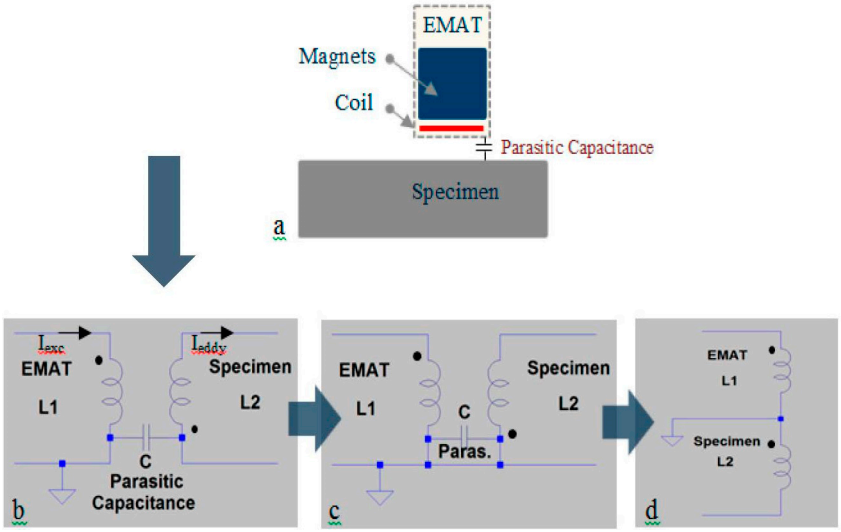

Figure 7. (**a**) Schematic of EMAT/specimen connection; (**b**) equivalent electrical circuit of EMAT/specimen without common ground connection; (**c**) common ground connection; (**d**) EMAT/specimen—autotransformer schematic.

Figure 8a shows the signal received from a defect-free area when the EMAT and the specimen do not have any common ground connection. In this figure the first reflection is the signal transmitted from the transmitter to the receiver and the other three are coming from the edges of the plate. In this case the noise level is high and the amplitude of all the reflections is low, leading to a low SNR.

Figure 8b illustrates the signal received when the defective area was tested without the common ground connection. Similar to Figure 8a, the signal transmitted and the three reflections from the edges of the plate are clearly obvious in the signal received. However, no reflections from the defect are obvious. Figure 9a demonstrates the signal received when the EMATs test the defect-free area while a common ground connection between the EMATs and the specimen has been established. In this case, the amplitude of the reflections increased, the noise level decreased, and as a result the SNR increased by five times. Figure 9b shows the signal received from the defective area when the EMATs and the specimen had a common ground connection. Similar to Figure 9a, the SNR of the signal increased four times more compared to the signal shown in Figure 8b. Actually, in Figure 9b both reflections from the crack are clearly obvious.

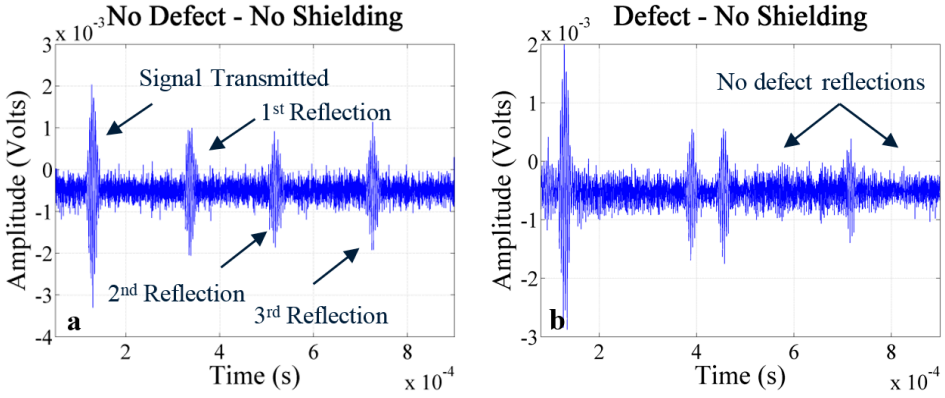

Figure 8. (**a**) Signal received from the defect-free area; (**b**) signal received from the defect.

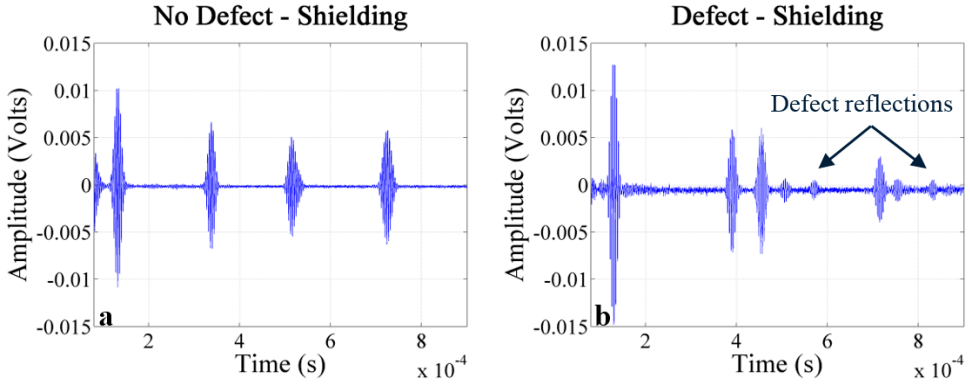

Figure 9. (**a**) Signal received from the defect-free area with shielding; (**b**) signal received from the defect with shielding.

Hence, the shielding has resulted in an enhanced SNR due to the noise cancellation. The electromagnetic coupling between the specimen and the EMAT receiver is weak when they are connected as a two-winding transformer (no shielding); in this case, the electromagnetic losses between the EMAT and the specimen are greater than in a conventional two-winding transformer, since no ferrite connects the EMAT and the specimen. The air between them increases the noise level and attenuates the electromagnetic coupling/"wanted" signal (there is no ferrite to drive the electromagnetic wave; on the contrary, the electromagnetic wave scatters when air is between the EMAT and the specimen). When the specimen/EMAT connection performs as an autotransformer, the

noise level decreases and the amplitude of the "wanted" signal (ultrasonic response of the specimen) increases; no noise interferes with the EMAT receiver and thus more current is induced to the coil. The autotransformer is more efficient than a two-winding transformer and as a result more current is induced in the coil when the autotransformer connection is established between the EMAT and the specimen. The unshielded EMAT has greater losses than a conventional transformer would have due to the weak connection between the EMAT and the specimen, while an autotransformer has smaller losses compared to both the unshielded EMAT and a conventional transformer. Thus, a significant increase in the amplitude of the "wanted" signal is observed when the EMAT is shielded. Consequently, the voltage difference between the EMAT and the specimen significantly affects the quality of the signal received and when there is no voltage difference and both components are connected to the ground, the probability of defect detection increases as well. Also, the frequency selected based on the size defect and the dispersion curves is proven to be correct for the detection of the 20 mm long defect.

The attenuation of the signal and the ToF of the main four reflections from the edges of the plate remain features that enable us to distinguish the defective from the defect-free areas when there was no common ground connection. Although the velocity of SH_0 was not to change during the experiments, for no temperature rise occurred, the ToF of both the first and the second reflection from the edges of the plate change from one case study to the other. It is likely that the defect causes this time delay by trapping a portion of the energy/spectrum of the wave propagating inside the plate.

From all the above figures and more especially from Figure 9a,b, it is obvious that only the SH_0 wave mode had been received from the EMAT; the time of arrival of the reflections matches with the SH_0 velocity, as it was calculated from the dispersion curves and the electromagnetic model. Hence, the experimental results match with the theoretical. However, further experimental investigation should be conducted regarding the wave purity characteristics of this EMAT design. In this set of experiments the EMAT receiver was mainly evaluated regarding its ultrasonic potentials; laser interferometry tests, during which the actual displacement generated from the EMAT transmitter can be observed, may also be required for further experimental evaluation of the EMAT transmitter regarding its wave purity characteristics.

Figure 10a illustrates how the amplitude of the signal transmitted changes (%) with respect to the lift-off. According to the literature, EMATs are sensitive to lift-off [28] and therefore their efficiency decreases with the increase of lift-off. The amplitude of the signal transmitted decreases almost linearly with the lift-off increase; when the lift-off is equal to 1 mm only the signal transmitted can be clearly observed. This confirms the high sensitivity of EMATs to lift-off; more particularly, the lift-off limitations of EMATs differ depending on the application the EMAT is designed for. EMATs for thickness measurements can still operate efficiently when the lift-off exceeds 1 mm; however, EMATs for guided waves are more sensitive to lift-off. A parameter that influences the performance of EMAT regarding lift-off is the impedance of the coil. The impedance changes with lift-off as well as with the material properties of the specimen. The inductance due to the magnetization of the specimen is smaller when the EMAT is employed on paramagnetic materials compared to ferromagnetic materials. Consequently, an alternative coil design should be used so that EMATs can be efficiently used in the inspection of absorber tubes, since the thickness of the glass envelope is 7 mm; stacked coils may be more efficient.

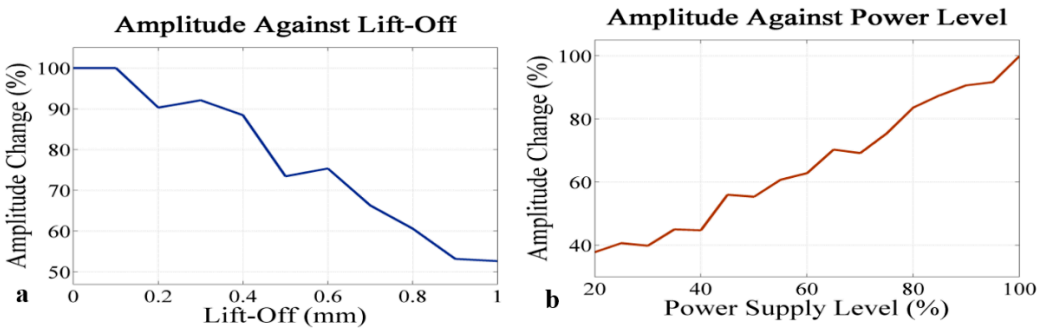

Figure 10. Amplitude change of signal transmitted against (**a**) lift-off increase; (**b**) power increase.

An experimental evaluation of these EMATs regarding their power requirements was also conducted. The power level decreased gradually from 100% to 20% with a step of 5%; we stopped there as no useful information could be retrieved from the signal received when the power level was smaller than 20%. Figure 10b shows how the amplitude of the signal transmitted increases with power supply increase; it can be observed that the amplitude increases almost linearly with the power increase. Similar to lift-off, the impedance of the coil affects the power requirements of EMATs. If the pulser/receiver unit drives the EMAT transmitter through an output resistor, the magnitude of the impedance of the coil should be equal to the output resistor of the pulser unit, so that the voltage drop in the coil will be minimized. Therefore, impedance matching is always required, which means that either a unit with zero output impedance should be chosen or an impedance matching network should be added between the pulser and the EMAT transmitter. Impedance matching should be used for the coil to be driven with the maximum power possible so that strong signals will be obtained. Nevertheless, the power supply level of EMATs remains high, leading to the conclusion that EMATs are considered to be more efficient as receivers rather than transmitters.

6.2. High-Temperature Experiments

As was mentioned in the theoretical section, high-temperature EMATs have been designed so far only for thickness measurements and thus an EMAT that can withstand high temperatures and excite guided waves is still required. A first approach for that would be the selection of the suitable high Curie magnets and high-temperature coil or the design of a cooling system so that the EMAT would be as efficient as possible at high temperatures. However, all of the above may result in a more complicated design. Hence, a further study about room temperature, guided wave EMATs, and their performance at high temperatures should be conducted prior to the design of a new EMAT.

Hence, the EMATs were tested from ambient temperature to 180 °C with a step of 10 °C; the maximum operating temperature of these EMATs is 250 °C and therefore they were tested up to 180 °C only, so that any serious and irreversible damage will be avoided. The EMATs were continuously exposed to the heat source with zero lift-off during the rise in temperature, while the overall time they were exposed to the heat was equal to 15 min. This set of experiments was conducted three times. Figure 11a–d show the signal received at room temperature, 60 °C, 100 °C, and 180 °C, respectively. Firstly, in the signal obtained at room temperature, both the reflections from the plate edges and the first two reflections from the defect are clear. However, it is obvious that the amplitude of the second reflection from the plate diminishes greatly after 60 °C, while at 100 °C and 180 °C it

can hardly be noticed. Similarly, the amplitute of the first reflection from the defect and the forth reflection from the plate decreases with the increase in temperature.

Figure 12 shows how the amplitude of the signal transmitted decreases with temperature rise; it is clear that the amplitute dwindles almost linearly with the rise in temperature. However, the amplitude of the signal transmitted in 30 °C and 40 °C was slightly larger than the amplitude at room temperature in the areas marked in red in Figure 12. Also, the amplitude error alters with temperature rise. A reason for that may be the ground connection between the EMAT and the specimen. The thermal conductivity of stainless steel is low and therefore the specimen was not heated up uniformly; as a result, the plate bended and the mechanical connection between the EMAT ground and the specimen altered with temperature rise due to the gradient of the bend. This mechanical/electrical connection significantly influences the amplitude of the signal transmitted and thus may be the reason for the amplitude increase at 30 °C and 40 °C.

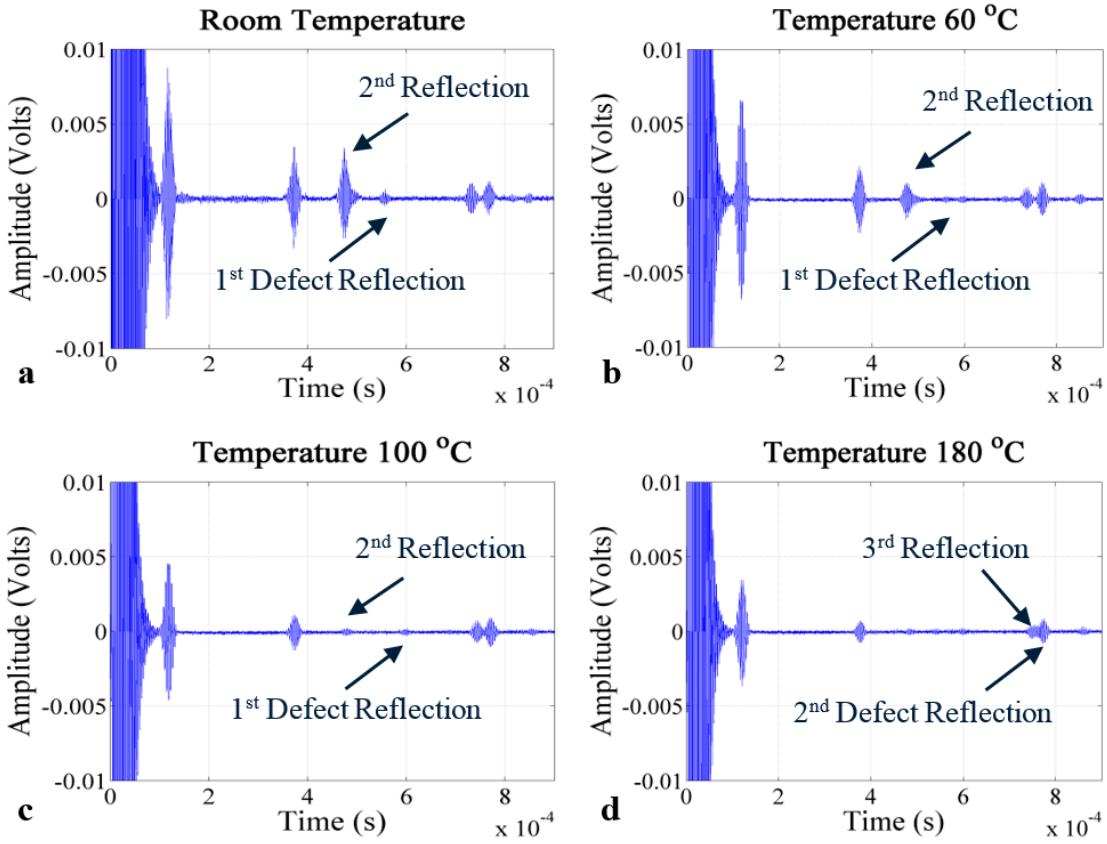

Figure 11. Signal received at (**a**) room temperature; (**b**) 60 ºC; (**c**) 100 ºC; (**d**) 180 ºC.

Time shifting is also observed, as was expected due to the change in the wave velocity at high temperatures, presented in the theoretical study. The third reflection from the plate shifts in time and starts coming closer to the second reflection from the crack, leading to an increase of the magnitude of the latter. Consequently, the experimental results match the theoretical. Temperature compensation should take place and both the ToF of the reflections as well as the drop of their amplitude may be two features that can be further processed and used for the identification of the temperature of the structure being tested. Room-temperature EMATs cannot be used for the monitoring of high-temperature structures (>100 °C); however, a high-temperature EMAT specifically designed for the monitoring of

high-temperature structures (>200 °C) should be compared with the performance of this EMAT up to 100 °C.

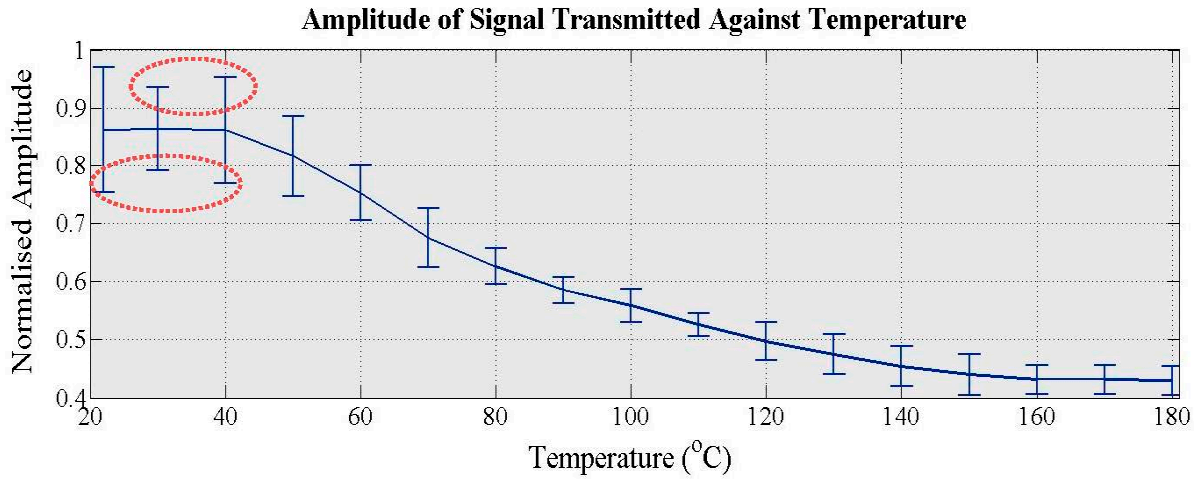

Figure 12. Amplitude of the signal transmitted against temperature.

7. Conclusions and Future Work

The absorber tube is an essential part of Parabolic Trough CSPs and is very likely to get damaged due to its hostile operating conditions. Hence, NDT techniques are required for their monitoring and/or inspection. A promising technique for this application is the use of high-temperature EMAT transducers for the excitation of guided waves and more particularly of the T(0,1) wave mode. A theoretical study about the GWT of absorber tubes, their dispersion curves, and the wave mode that should be applied for their inspection were calculated. The ultrasonic response of a PPM EMAT and its wave purity characteristics were also presented. A pair of PPM EMATs was experimentally evaluated regarding its wave purity, its sensitivity to noise, its lift-off limitations, its power requirements, and its performance at high temperatures while it was exciting/receiving guided waves. It was found that a PPM EMAT receiver can mainly detect SH_0 and thus it can be used for the GWT of the absorber tubes in terms of wave purity characteristics, as the theoretical study also showed. However, laser interferometry tests are also required for the transmitter to be validated. Also, a common ground connection between the EMAT and the specimen can significantly enhance the SNR of the signal received. The current EMAT design is not efficient enough to inspect a stainless steel pipe with a lift-off larger than 1 mm and therefore it cannot be employed for the inspection of absorber tubes. A room-temperature EMAT cannot be applied at high temperatures (<200 °C) and thus a high-temperature EMAT is still required for the guided wave monitoring of high-temperature structures.

The design and manufacturing of a high-temperature PPM EMAT with racetrack coil operating efficiently at temperatures higher than 300 °C for long-term inspection or monitoring is our next step. Several thermal, electromagnetic, and mechanical simulations have already been carried out and have given encouraging results. Moreover, a further experimental investigation regarding the impedance of the EMAT and its relationship with the lift-off and the material properties of the specimen being tested is also another part of our future research.

Acknowledgments

The authors are indebted to the European Commission for the provision of funding through the INTERSOLAR FP7 project. The INTERSOLAR project is coordinated and managed by Computerized Information Technology Limited and is funded by the European Commission through the FP7 Research for the benefit of SMEs program under Grant Agreement Number: GA-SME-2013-1-605028. The INTERSOLAR project is a collaborative research project between the following organizations: Computerized Information Technology Limited, PSP S.A., Technology Assistance BCNA 2010 S.L., Applied Inspection Limited, INGETEAM Service S.A., Brunel University, Universidad De Castilla—La Mancha (UCLM), and ENGITEC Limited.

Author Contributions

M.K. performed the literature review and the finite element simulations, conducted all the experiments and wrote the paper; A.M., V.K. and C.S. reviewed the manuscript; T.-H.G., W.B. and L.C. supervised the research.

Conflicts of Interest

The authors declare no conflict of interest.

References

1. Poullikkas, A. Economic analysis of power generation from parabolic trough solar thermal plants for the Mediterranean region—A case study for the island of Cyprus. *Renew. Sustain. Energy Rev.* **2009**, *13*, 2474–2484.
2. Staff, C.W. Industry Experts Trumpet Untold Solar Potential. 2013. Available online: http://www.constructionweekonline.com/article-23701-industry-experts-trumpet-untold-solar-potential/ (accessed on 12 March 2015).
3. Taggart, S. Parabolic troughs: Concentrating Solar Power (CSP)'s Quiet Achiever. 2008. Available online: http://www.renewableenergyfocus.com/view/3390/parabolic-troughs-concentrating-solar-power-csp-s-quiet-achiever (accessed on 12 March 2015).
4. Steinfeld, A. Topics for Master/Bachelor Thesis and Semester Projects: Spectral Optical Properties of Glass Envelopes of Parabolic trough Concentrators. Available online: http://www.pre.ethz.ch/teaching/topics/?id=87 (accessed on 18 August 2015).
5. Guillot, S.; Faika, A.; Rakhmatullina, A.; Lambert, V.; Verona, E.; Echegut, P.; Bessadaa, C.; Calvet, N.; Py, X. Corrosion effects between molten salts and thermal storage material for concentrated solar power plants. *Appl. Energy* **2012**, *94*, 174–181.
6. Herrmann, U.; Kearney, D.W. Survey of Thermal Energy Storage for Parabolic Trough Power Plants. *J. Sol. Energy Eng.* **2002**, *124*, 145–152.
7. Papaelias, M.; Cheng, L.; Kogia, M.; Mohimi, A.; Kappatos, V.; Selcuk, C.; Constantinou, L.; Muñoz, C.Q.G.; Marquez, F.P.G.; Gan, T.H. Inspection and structural health monitoring techniques for concentrated solar power plants. *Renew. Energy* **2015**, *85*, 1178–1191.

8. Lee, J.L.; Hu, L.W.; Saha, P.; Kazimi, M.S. Numerical analysis of thermal striping induced high cycle thermal fatigue in a mixing tee. *Nucl. Eng. Des.* **2009**, *239*, 833–839.
9. Noguchi, Y.; Okada, H.; Semba, H.; Yoshizawa, M. Isothermal, thermo-mechanical and bithermal fatigue life of Ni base alloy HR6W for piping in 700 °C USC power plants. *Procedia Eng.* **2011**, *11*, 1127–1132.
10. Jinu, G.R.; Sathiya, P.; Ravichandran, G.; Rathinam, A. Comparison of thermal fatigue behaviour of ASTM A 213 grade T-92 base and weld tubes. *J. Mech. Sci. Technol.* **2010**, *24*, 1067–1076.
11. Sunny, S.; Patil, R.; Singh, K. Assessment of thermal fatigue failure for BS 3059 boiler tube experimental procedure using smithy furnace. *Int. J. Emerg. Technol. Adv. Eng.* **2012**, *2*, 391–398.
12. Posteraro, K. Thwart Corrosion under Industrial Insulation. *Chem. Eng. Prog.* **1999**, *95*, 43–47.
13. Halliday, M. Preventing corrosion under insulation-new generation solutions for an age old problem. *J. Prot. Coat. Linings* **2007**, *24*, 24–36.
14. De Vogelaere, F. Corrosion under insulation. *Process. Saf. Prog.* **2009**, *28*, 30–35.
15. Kumar, M.S.; Sujata, M.; Venkataswamy, M.A.; Bhaumik, S.K. Failure analysis of a stainless steel pipeline. *Eng. Fail. Anal.* **2008**, *15*, 497–504.
16. Stine, W.B.; Harrigan, R.W. *Solar Energy Systems Design*; John Wiley and Sons, Inc.: New York, NY, USA, 1986.
17. Hutchins, D.A.; Saleh, C.; Moles, M.; Farahbahkhsh, B. Ultrasonic NDE Using a Concentric Laser/EMAT System. *J. Nondestruct. Eval.* **1990**, *9*, 247–261.
18. Kirk, K.J.; Lee, C.K.; Cochran, S. Ultrasonic thin film transducers for high-temperature NDT. *Insight* **2005**, *47*, 85–87.
19. Momona, S.; Moevus, M.; Godina, N.; R'Mili, M.; Reynauda, P.; Fayolle, G. Acoustic emission and lifetime prediction during static fatigue tests onceramic-matrix-composite at high temperature under air. *Compos. A Appl. Sci. Manuf.* **2010**, *41*, 913–918
20. Shen, G.; Li, T. Infrared thermography for high temperature pipe. *Insight* **2007**, *49*, 151–153.
21. Beattie, G. Acoustic emission principles and instrumentation. *J. Acoust. Emiss.* **1983**, *2*, 95–128.
22. Hagemaier, D.J. *Fundamentals of Eddy Current Testing*; American Society for Nondestructive, Testing: Columbus, OH, USA, 1990.
23. Malmo, J.T.; Jøkberg, O.J.; Slettemoen, G.A. Interferometric testing at very high temperatures by TV holography (ESPI). *Exp. Mech.* **1998**, *28*, 315–321.
24. Silk, M.G.; Bainton, K.F. The propagation in metal tubing of ultrasonic wave modes equivalent to Lamb waves. *Ultrasonics* **1979**, *17*, 11–19.
25. Pfander, M.; Lupfert, E.; Pistor, P. Infrared temperature measurements on solar trough absorber tubes. *Sol. Energy* **2007**, *81*, 629–635.
26. Cawley, P.; Alleyne, D. The use of Lamb waves for the long range inspection of large structures. *Ultrasonics* **1996**, *34*, 287–290.
27. Hirao, M.; Ogi, H. A SH-wave EMAT technique for gas pipeline inspection. *NDT E Int.* **1999**, *32*, 127–132.
28. Bottger, W.; Schneider, H.; Weingarten, W. Prototype EMAT system for tube inspection with guided ultrasonic waves. *Nucl. Eng. Des.* **1986**, *102*, 369–376.

29. Wilcox, P.; Lowe, M.; Cawley, P. Omnidirectional guided wave inspection of large metallic plate structures using an EMAT array. *IEEE Trans. Ultrason. Ferroelectr. Freq. Control* **2005**, *52*, 653–665.
30. Andruschak, N.; Saletes, I.; Filleter, T.; Sinclair, A. An NDT guided wave technique for the identification of corrosion defects at support locations. *NDT E Int.* **2015**, *75*, 72–79.
31. Burrows, S.E.; Fan, Y.; Dixon, S. High temperature thickness measurements of stainless steel and low carbon steel using electromagnetic acoustic transducers. *NDT E Int*. **2014**, *68*, 73–77.
32. Hernandez, V.F. Pulsed-Electromagnet EMAT for High Temperature Applications. Ph.D. Thesis, University of Warwick, Warwick, UK, 2011.
33. Idris, A.; Edwards, C.; Palmer, S.B. Acoustic wave measurement at elevated temperature using a pulsed laser generator and an Electromagnetic Acoustic Transducer detector. *Nondestruct. Test. Eval.* **1994**, *11*, 195–213.
34. Dixon, S.; Edwards, C.; Palmer, S.B. High-accuracy non-contact ultrasonic thickness gauging of aluminium sheet using electromagnetic acoustic transducer. *Ultrasonics* **2001**, *39*, 445–453.
35. Jian, X.; Dixon, S.; Edwards, R.S.; Morrison, J. Coupling mechanism of an EMAT. *Ultrasonics* **2006**, *44*, 653–656.
36. Ribichini, R.; Cegla, F.; Nagy, P.B.; Cawley, P. Study and Comparison of Different EMAT Configurations for SH Wave Inspection. *IEEE Trans. Ultrason. Ferroelectr. Freq. Control* **2011**, *58*, 2571–2581.
37. Gaultier, J.; Mustafa, V.; Chahbaz, A. EMAT Generation of Polarized Shear Waves for Pipe Inspection. In Proceeding of the 4th PACNDT, Toronto, ON, Canada, 14–18 September 1998.
38. Rose, J.L.; Lee, C.M.; Hay, T.R.; Cho, Y.; Park, I.K. Rail Inspection with Guided Waves. In Processing of the 12th A-PCNDT—Asia-Pacific Conference on NDT, Auckland, New Zealand, 5–10 November 2006.
39. Jackel, P.; Niese, F. EMAT Application: Corrosion Detection with Guided Waves in Rod, Pipes and Plates. In Proceedings of the 11th European Conference on Non-Destructive Testing (ECNDT 2014), Prague, Czech, 6–10 October 2014.
40. Hübschen, G. Generation of Horizontally Polarized Shear Waves with EMAT Transducers. *e-J. Nondestruct. Test.* **1998**, *3*, 1–7.
41. Kogia, M.; Mohimi, A.; Liang, C.; Kappatos, V.; Selcuk, C.; Gan, T.H. High temperature Electromagnetic Acoustic Transducer for the inspections of jointed solar thermal tubes. In Proceedings of the First Young Professionals International Conference, Budapest, Hungary, 17–20 September 2014.
42. Pulse Electronics, Understanding Common Mode Noise. Available online: www.pulseelectronics.com/download/3124/g204/pdf (accessed on 10 November 2015).
43. Winders, J. Autotransformers and Three-Winding Transformers. In *Power Transformers: Principles and Applications*; 1st ed.; Marcel Dekker: New York, NY, USA, 2002.